

Numerical Computational Technique for Scattering from Underwater Objects

T. Ratna Mani, Raj Kumar* and O.Vijay Kumar

Naval Physical and Oceanographic Laboratory, Cochin

**Defence Institute of Advanced Technology, Pune*

E-mail: ratna_mani51@yahoo.com

ABSTRACT

This paper presents a computational technique for mono-static and bi-static scattering from underwater objects of different shape such as submarines. The scatter has been computed using finite element time domain (FETD) method, based on the superposition of reflections from the different elements reaching the receiver at a particular instant in time. The results calculated by this method has been verified with the published results based on ramp response technique. An in-depth parametric study has been carried out, by considering different pulse frequency, pulse length, pulse type (CW, LFM, SFM), sampling frequency, as well as different size, shape of the scattering body and grid size. It has been observed that increasing the pulse frequency, sampling frequency and number of elements leads to improved results. However, good amount of accuracy has been achieved with element size less than one third of wave length. The experimental result of the underwater object has been found very close to the simulated result. This technique is useful for computing forward scatter for inverse scattering applications and as well as to generate forward scatter of very narrow and wide band signals of any pulse type and shape of body.

Keywords: Mono-static, bi-static, acoustic wave, scattering, finite element time domain method and ramp response technique

1. INTRODUCTION

Underwater acoustic imaging techniques and inverse analysis of acoustic scattering have many important applications such as shape reconstruction, size estimation, identification and classification of underwater objects. Inverse scattering is acquiring the size and shape of the underwater object, without a priori knowledge of the object by using the data obtained by direct scatter from the body or by computing the forward scatter. Forward scattering involves determining the amplitude and phase of the scatter field from the underwater object. Computational methods developed for forward scatter are mostly analytical. The choice of the computation method depends on the signal frequency, type of object to be examined and the application of the simulated scatter viz. shape reconstruction, size estimation, identification/classification of the object. Mathematically, the approaches rely on integral formulations of the Helmholtz equation and with appropriate boundary conditions. In open literature several research papers have reported on scattering from underwater objects, for the application of analysing underwater imaging techniques.

Young¹ presented a new method to generate the 3-D image of objects from the ramp response, which is called 'approximate limiting surface' technique. Zhang², *et al.* developed a numerical method to obtain the ramp response for underwater objects in acoustic field, which requires limited data of frequency domain. A method for obtaining size and shape of the object using back scattered data in the high frequency was also reported³. The T-matrix method was originally introduced by Waterman⁴⁻⁵

as a method for systematically solving the acoustic scattering problem of arbitrarily convex shaped targets with Neumann or Dirichlet boundary. Varadan⁶, *et. al.* extended the T-matrix method to the elastic wave scattering field, and this is the method employed in generating back scatter for identifying size of the object³. Size of the object is identified by low frequency information from the broad band information, while high frequency information is more important in identification of shape of the object.

The impulse response technique was introduced by Kennough⁷ for computing forward scatter and generally employed in inverse scattering applications. The analytical methods based on impulse response techniques have limited practical applications as the wide band returns from the underwater body are also highly influenced by media.

However, present trends in target strength computations are based on finite element method (FEM) and boundary element method (BEM), that are numerical methods⁸. The FEM and BEM methods are used in target strength computations. These can be applied for forward scattering computation as they can handle the fluid - body interactions. The extension of FEM has been applied to data simulation in forward scattering that is required in inverse applications. The limitations of these methods can be overcome by using the finite element time domain (FETD) method. This method is used in simulation of data for biomedical applications for velocity change which depends on density changes, but not for underwater applications¹². So far, much work has not been

reported in open literature based on finite element time domain (FETD) method particularly to simulate the forward scatter for underwater objects. This method is versatile to simulate back scatter for very narrow band as well as broad band, and any type of pulse signal. This method can also be applied efficiently to any arbitrary shape of scattering body and for mono-static as well as bi-static modes.

In this paper, FETD method has been developed and applied to compute the scattering signal from an underwater object, as time series similar to data that collected in practical applications. The simulated time series is helpful for analyzing the inverse scattering techniques. The scattering information has been computationally obtained for mono-static, bi-static mode at different frequencies and pulse length, etc. The simulation is based on plane wave approximation. Shape extracted by computing the profile function, from the computed scatter, is very close to the shape of the back scattering object selected for simulation. The time series computed of this method is found in very close agreement to experimental results.

2. APPROACH FOR SCATTERING COMPUTATION

A number of approaches for calculating scattering are available in literature^{3,12,13}. The approach Krichhoff approximation is based on ray acoustics and the plane wave approximation (PWA) that is derived from radiation problem are described here⁸.

2.1. Basics

First, we consider the acoustic wave equation

$$p,_{ii} - \frac{1}{c^2} p,_{tt} = 0, \quad (1)$$

with subscripts i and t denoting the spatial and temporal differentiation. Fourier transformation leads to the elliptic Helmholtz equation

$$p,_{ii} + k^2 p = 0, \quad (2)$$

where c is the speed of sound and k is the wave number $k = \omega/c$ with circular frequency ω . Equation (2) can also be written as

$$\Delta p(\bar{x}) + k^2 p(\bar{x}) = 0; \quad \bar{x} \in \mathbb{R}^3 \quad (3)$$

the time harmonic form:

$$p = \hat{p}e^{i\omega t}; \quad \hat{p} \in \mathbb{C} \quad (4)$$

is used. This causes a Fourier transformation of the form:

$$\int_{-\infty}^{+\infty} f(t)e^{-j\omega t} \quad (5)$$

Following this notation we obtain the fundamental solution or the Green's function in free space of Eqn (2) as

$$g,_{ii} + k^2 g = -\delta(X, rP)g(X, rP) = \frac{e^{-ikr}}{4\pi r} \quad (6)$$

where δ is the Dirac function, r is the Euclidean distance between the load point $\bar{r} P$

And the field point $\bar{X}(r = |\bar{X} - \bar{r}p|)$ and $\bar{r} p$ is located on the boundary Γ (Fig. 1).

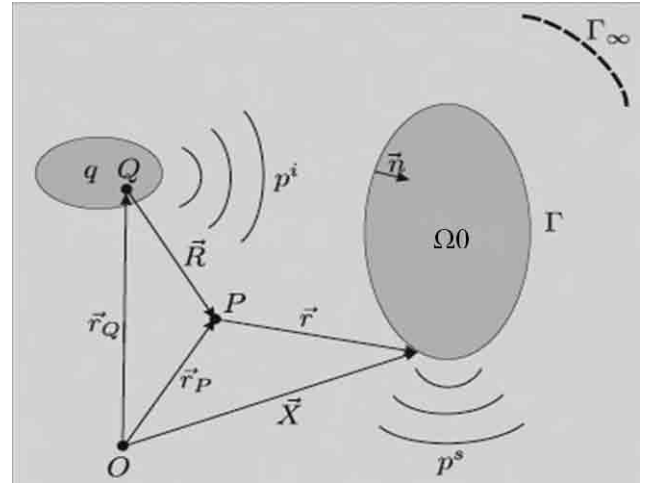


Figure 1. Domain Ω including source Q and scatterer Ω_0 .

2.2 High Frequency Approach by Means of Kirchhoff Approaches (for first order)

In BEM approach, a coupled system of equations has to be solved which usually means the inversion of a large matrix. In the high frequency range a BEM approach fails because of limited computer memory or limited computer time.

To obtain the integral equation for the scattered sound field one can also take a look at the Helmholtz integral equation just for the scattered sound field p^s for an exterior problem, which results in

$$C(P)p^s(P) = -\int_{\Gamma} g_i \omega q v_n + p^s \frac{\partial g}{\partial n} d\Gamma \quad (7)$$

Imagine that the obstacle is not existent. The interior integral formulation just for the incident wave p^s obtained from the sound source in the absence of the obstacle can be written as

$$C^0(P)p^s(P) = -\int_{\Gamma} g_i \omega q v_n + p^s \frac{\partial g}{\partial n} d\Gamma \quad (8)$$

where C^0 is the complimentary surface integral to C subtraction of Eqn (7) from Eqn (6) and making use of the superposition of scattered and incident field similar to that in optics

$$p_n = p^i + p^s = 0, \quad v_n = v_n^i + v_n^s = 0 \quad (9)$$

and $C + C^0 = 1$

for $P \in \Omega$ leads to

$$p^s(P) = \int_{\Gamma} g_i \omega q v_n + p \frac{\partial g}{\partial n} d\Gamma \quad (10)$$

However, in the high frequency region one can accept some simplifying assumptions to avoid the explicit process of solving a system of equations. This leads to an approach, which is comparable with a BEM-field point calculation.

The first assumption is that the boundary Γ is divided into a part that is illuminated Γ_{ill} (visible) and another, which is non illuminated Γ_{nonill} (nonvisible) by the source or in the bi-static case, resp. by the receiver. The boundary integration procedure is now reduced to the illuminated part only. Another assumption is the use of a given reflection coefficient $R \in \mathbb{C}$ on the boundary Γ_{ill} , so that the scattered sound field can be written as

$$p^s = Rp^i \quad (11)$$

The gradient in normal direction on this boundary is

$$\frac{\partial p^s}{\partial n} = -R \frac{\partial p^i}{\partial n} \quad (12)$$

$$\text{As } \frac{\partial p}{\partial n} = -i\omega qv_n$$

$$p^s(P) = \iint_{\Gamma_{\text{ill}}} \left[(1-r)g \frac{\partial p^i}{\partial n} - (1+r)p^i \frac{\partial g}{\partial n} \right] d\Gamma, \quad P \in \Omega \quad (13)$$

2.3. Plane Wave Approximation

The plane wave approximation (PWA) was originally only used for radiation and not for scattering problems¹¹. In the high-frequency range, it is assumed that pressure and normal velocity on the surface of the radiator are satisfying

$$p = \rho cv_n, \quad (14a)$$

if the normal is directed into the exterior domain or

$$p = -\rho cv_n, \quad (14b)$$

if the normal is directed into the interior domain.

This PWA is only true, if several conditions are satisfied.

- First, the wavelength has to be small compared with the radius of curvature of the radiating surface.
- Second, the wavelength must also be smaller than the size of those areas of the surface, which are scattered sound pressure p^s in the exterior domain Ω vibrating in phase.
- Third, the surface of the radiator should be convex, so that the radiated sound field is not back-scattered by parts of the radiator itself.

In other words, multiple reflections are not allowed.

Considering the integral equation for the scattered sound field p^s for an exterior problem

The integral equation for the scattered sound pressure p^s in the exterior domain Ω

$$p^s(P) = -\int_{\Gamma} \int \left[\frac{\partial p^s}{\partial n} g - p^s \frac{\partial g}{\partial n} \right] d\Gamma, \quad P \in \Omega \quad (15)$$

or the equivalent integral Eqn (10) containing the total quantities

$$p_n = p^i + p^s = 0 \text{ and } v_n = v_n^i + v_n^s = 0 \quad (16)$$

$$p^s(P) = -\int_{\Gamma} \int \left[\frac{\partial p}{\partial n} g - p \frac{\partial g}{\partial n} \right] d\Gamma, \quad P \in \Omega \quad (17)$$

which is obtained by adding Eqn (15) and the interior integral formulation for the incident wave Eqn (7).

Where Ω is the set of discretised elements of the structure and $d\Gamma$ is corresponding to space discretization and δg is the normal derivative of the greens function.

2.3.4 Rigid Case

For simplicity, first consider the case where the surface of the scattering body is rigid, and hence the total normal surface velocity vanishes all over the surface:

$$v_n = v_n^i + v_n^s = 0$$

Equivalently, $(\partial p/\partial n) = 0$, and therefore, the integral Eqn (16) for the total field quantities reduces to

$$p^s(P) = -\int p \frac{\partial g}{\partial n} d\Gamma, \quad P \in \Omega \quad (18)$$

For obtaining an approximation for the yet unknown total pressure $p = p^i + p^s$, we need an estimation for the scattered pressure. Due to the boundary condition Eqn (17), the scattered normal velocity on the surface is given by $v_n^s = -v_n^i$. Thus the scattering problem can be interpreted as an equivalent radiation problem as follows¹⁰:

If the structure is assumed to vibrate with the negative normal velocity $-$, the radiated sound pressure is identical to the pressure p^s scattered from Ω_0 due to the incident wave p^i . Now, we are able to apply the PWA Eqn (14(b)) for finding a relationship between scattered pressure and normal velocity by assuming that in the high frequency range

$$p^s = -\rho cv_n^s = -\rho c - (v_n^i) = \rho cv_n^i \quad (19)$$

By substituting assumption Eqn (19) into Eqn (18), we immediately obtain

$$p^s(P) = -\int_{\Gamma} \int (p^i + \rho cv_n^i) \frac{\partial g}{\partial n} d\Gamma, \quad P \in \Omega \quad (20)$$

Equation (20) is the PWA for the pressure scattered from a rigid structure by an incident wave p^i . Clearly, the advantage of this approximation is that the scattered pressure can be calculated only by an integration over the surface of the scatterer. Thus, there is no need to solve an integral equation or a linear system of equations for a discretized structure.

Now compare the PWA for scattering and the Kirchhoff approach of first order as described earlier. There are several slightly different representations of the Kirchhoff approximation in the literature. Originally, the approach was suggested by Kirchhoff for treating the diffraction of light when passing through apertures.

For acoustics, the same procedure is explained⁹, if there is an aperture D . However, the total sound pressure on the screen depends on the boundary condition on the screen. For example, if the screen, which can be identified with the scattering object, is rigid, the reflection coefficient R becomes 1, and hence a suitable approximation would be to assume that the pressure on the boundary is twice the incident pressure, just as it occurs in the Rayleigh integral. Considering this fact into

Account

$$p^s = Rp^i \text{ and } \frac{\partial p^s}{\partial n} = -R \frac{\partial p^i}{\partial n} \quad (21)$$

Inserting Eqn (21) into Eqn (16) and performing the surface integral only over the illuminated part Γ_{ill} of the surface Γ , which means that $(e_{in}, n) > 0$, we get Eqn (20)

$$p^s(P) = -\int_{\Gamma_{\text{ill}}} \int \left[(1-R)g \frac{\partial p^i}{\partial n} - (1+R)p^i \frac{\partial g}{\partial n} \right] d\Gamma \quad (22)$$

and for $R = 1$, we obtain

$$p^s(P) = -2 \iint_{\Gamma_{\text{ill}}} \left[p^i \frac{\partial g}{\partial n} \right] d\Gamma, \quad P \in \Omega \quad (23)$$

By comparing Eqns (20) and (23), it can be seen that the Kirchhoff approach and the PWA becomes equal if two conditions are fulfilled:

- (1) $p^i = \rho c v_n^i$
- (2) The integration is only performed over the illuminated part of the scatterer.

However, the first assumption $p^i = \rho c v_n^i$ is only true, if an incident plane wave is considered, where the normal vector n of the scattering surface is parallel to the unit normal vector in the incidence direction of the incident wave e_{in} . Clearly, this is only the case for perpendicular incidence. Thus, if the PWA is restricted to the case of incident plane waves, we obtain

$$p^s(P) = - \iint_{\Gamma_{\text{ill}}} \left[p^i (1 + (e_{in}, n)) \frac{\partial g}{\partial n} \right] d\Gamma,$$

In summary, the kirchhoff approximation and the PWA are leading to the same result, equivalent to that of simple BEM for high frequency, if first the incident wave is a plane wave, second, only the illuminated part of the surface is considered, and third, the variation of the reflection coefficient with the angle of incidence is neglected. This also hence scattering with PWA has been selected for computation of time series forward scatter waveform.

In short, considering the case where the surface of the scattering body is rigid and reference to Fig. 1 valid scattering formulation of Eqn (20)

$$P^s(P) = - \int_{\Gamma} \int (p^i + c v_n^i) \delta g / \delta n d\Gamma \quad P \in \Omega \quad (24)$$

Equation (24) is the PWA for the pressure scattered from a rigid structure by an incident wave p^i considering reflection coefficient $R=1$, for rigid structure

$$P^s(P) = - \iint_{\Gamma_{\text{ill}}} (p \delta g d\Gamma / \delta n) \quad P \in \Omega \quad (25)$$

Equation (25) is the pressure scattered from the illuminated area from Eqn (23). The above method is extended for simulation of time series of forward scatter in free field.

3. FINITE ELEMENT TIME DOMAIN METHOD

In formulating the finite element time domain method (FETD) method, the signal at the receiver in time domain, is a sequence formed by integral over the scattered pressure, at that time-instance of the sequence. For a given object as shown in Fig. 2. as the wave reaches the element, it is a function of sound velocity, transmission angle θ_t , grid size and element number. The scattered wave that reaches the receiver is also a function of sound velocity, receiver angle θ_r , grid size and element number.

Assuming sound speed as constant (c) and defining the grid as

X : - $(N/2 - 1) d$: $(N/2 - 1) d$, vector of size N

Y : - $(M/2 - 1) d$: $(M/2 - 1) d$, vector of size M

For given transmission angle (θ_i, Φ_r) , the time delay (vector of $N \times M$) due to incident is given by

$$T_i = (X \cos(\theta_i) + Y \sin(\Phi_r)) / c$$

Similarly, for given receiver angle (θ_r, Φ_r) , the time delay (vector of $N \times M$) due to receiver is given by

$$T_r = (X \cos(\theta_r) + Y \sin(\Phi_r)) / c$$

The total time, an incident impulse reaches the receiver from different elements

$$T = T_i + T_r \text{ (vector } N \times M)$$

For the transmitted signal $\sin(\omega t)$, the signal at the receiver at time t^n is, $[\sin\{\omega(t^n - T_{mn})\}]$ from each element. For a given angle θ_r , source assumed to be on the normal of the objects plane Φ_r computed by the size of the object.

The received signal from each element can thus be computed by using the total delay for that element. The incident wave is explicitly specified as a Dirichlet condition updated at each time step. The wave reflected by the scatter is dependent on the time the incident wave reaching the discretised element as well as area of the element. The phase of the wave is dependent on time it reaches the element. Relative time of the wave from different elements depends on the relative distance travelled by the wave with respect to the first element. This is dependent on the angle of transmission (θ) also. In a similar way the signal received is also time dependent and decided by the receiver angle (θ_r). Discretising the time t by high sampling rate, at n^{th} time instance (t^n) a number of reflected signals from different elements arrives at the receiver. Therefore the signal at the receiver, at n^{th} time instance (t^n) is integral of scattered pressure from different elements reaching the receiver at that time instance. Replacing the integral

$$R^s(t^n) = \sum_p (P^s(P))_{t^n} \quad (26)$$

where $P^s(P)$ is given by Eqn (25)

The time series formed by the concatenation of the $R^s(t^n)$ in time. With appropriate modification for mono-static and bi-static modes, and suitably selecting the number of elements and the sampling frequency, the received data are simulated. The verification of results was carried out by obtaining the object shape through ramp response technique, on the simulated time series.

The profile of the body is estimated

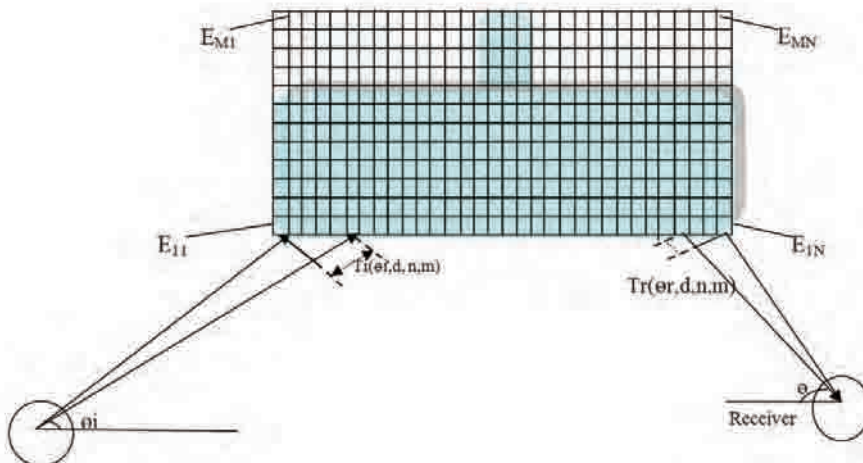


Figure 2. Finite element grid of the object and time delay.

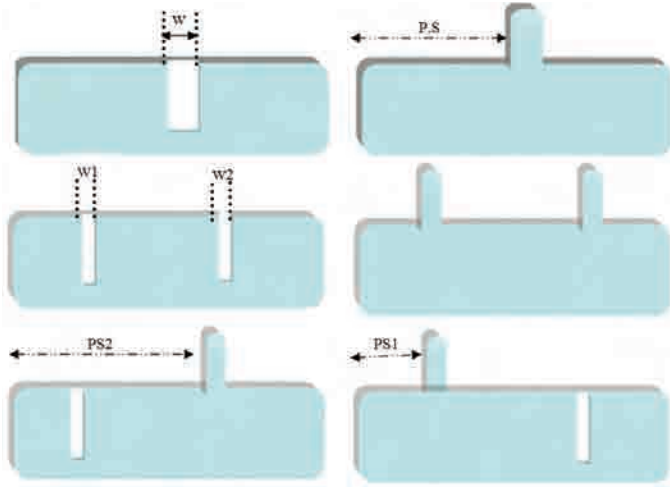


Figure 3. 2D shapes used for simulation of scatter from underwater objects.

by ramp response and given as second integral of the impulse response²⁶. This is given by

$$P_R(t) = \int \int P_i(t'') dt'' dt \quad (27)$$

Equation (27) is used for extracting the profile function.

The ramp response technique can also be applied for profile extraction with the band limited signal¹³. The object shapes simulated are illustrated shown in Fig. 3. Different combinations of projections and depressions on the body were simulated to study the effect of frequency and pulse length on the feature size. For the verification of the computed scatter, the method is applied on the object type half buried spheroid¹⁴. Fig. 1(a) time series calculated for half buried spheroid and Fig. 1(b) is the shape extracted from the simulated time series

4. RESULTS AND DISCUSSION

The 2D underwater object selected for scattering is shown in Fig. 3. The forward scatter of object has been simulated using FETD method for single cycle for different frequencies. The profile function was obtained by using ramp response technique¹³. The shape of results obtained using profile function¹³ is very close to the object shape selected for scatter computation by FETD method. The several object shapes were used in simulations for scatter. The computation are carried out for different pulse parameters, size of the objects, as well as different sizes of the spatial grid and sampling frequencies. The parameters used in simulation are i.e. frequency; 25 KHz, transmitter angle $\theta_i = 85^\circ$ and receiver angle $\theta_r = 85^\circ$. The other parameters are taken like number of cycles, number of finite elements 500×50 , Element type rectangular; size of the body; 10×1 meters and sound velocity = 1500 m/s.

4.1 Mono-static Mode

In Fig. 3, a rectangular body is defined as the basic shape and another rectangle/triangle is either added or subtracted to obtain the desired shape. The parameters like, placement of the alteration (P.S), width of the shape (w), and alteration type (a+ or a-) are described along with the result. Figs. 5 to 9 indicates the time series generated and profile function extracted for mono-static case. Fig. 5(a) denotes time series from simulation for P.S = 200, w = 10, type = a- and number

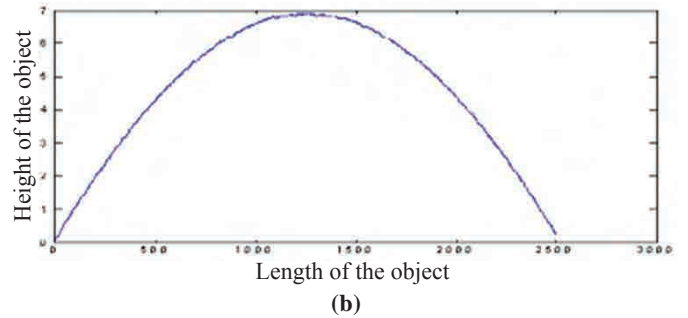
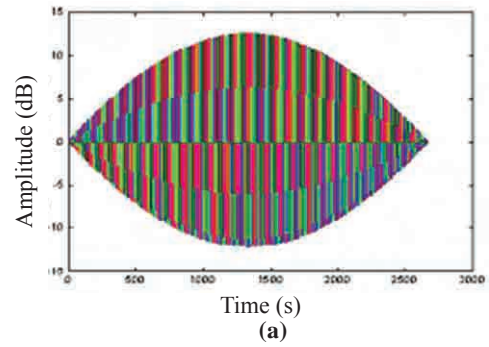


Figure 4. (a) Time series from simulation, (b) Profile function from Fig 1(a).

of cycles = 1. Fig. 5(b), denotes corresponding profile functions extracted from time series generated in Fig. 5(a). Fig. 6(a) shows the time series simulated for P.S = 200, w = 10, type = a+ and number of cycles = 3. And Fig. 6(b) presents the profile function extracted from Fig. 6(a). In Fig. 7(a) exhibits the time series from simulation for type = a- and number of cycles = 13 and mono-static profile function extracted from Fig. 7(a) is shown in Fig. 7(b). It is observed that with very narrow pulse, the time series generated clearly indicates the modulation of the signal by the shape of the object and the profile extracted is very close to the object shape. The effect of pulse width is seen as elongation of the feature shape and length of the time series shown in Fig. 7. The profile extracted indicates the shape of the object. For the Figs. 5(a) to 9(a), the 'x-axis' corresponds to time ($10 \mu\text{s}/\text{sample}$, re-sampled by a factor of 10), given as sample number and 'y-axis' corresponds to amplitude (mill volts) if the signal at the receiver. For the Figs 5(b) to 9(b), the 'x-axis' corresponds to length of the object ($7.5 \text{ mm}/\text{sample}$ re-sampled by a factor of 10), given as sample number and 'y-axis' corresponds to the height of the object.

4.2 Bi-static Mode

Bi-static mode has elongated the feature size and the time series as shown in Figs. 8(a) and 9(a). The Profile extracted indicates the shape of the object shown in Figs. 8(b) and 9(b). In bi-static case, the time series from simulation has been taken for the shape parameters P.S = 200, w = 10, type = a+ number of cycles = 20 with the transmission angle $\theta_i = 85^\circ$ and receiver angle $\theta_r = 45^\circ$. In Fig. 8(b), the profile extracted indicates the shape of the object. The profile extracted in bi-static shown in Fig. 9(b) has been calculated from the time series for shape parameters P.S₁ = 1000, w₁ = 100, type1 = a+ number P.S₂ = 1000, w₂ = 100, type2 = a- number of cycles = 20, Transmission angle $\theta_i = 5^\circ$ and receiver angle $\theta_r = 60^\circ$. However, the grid size was

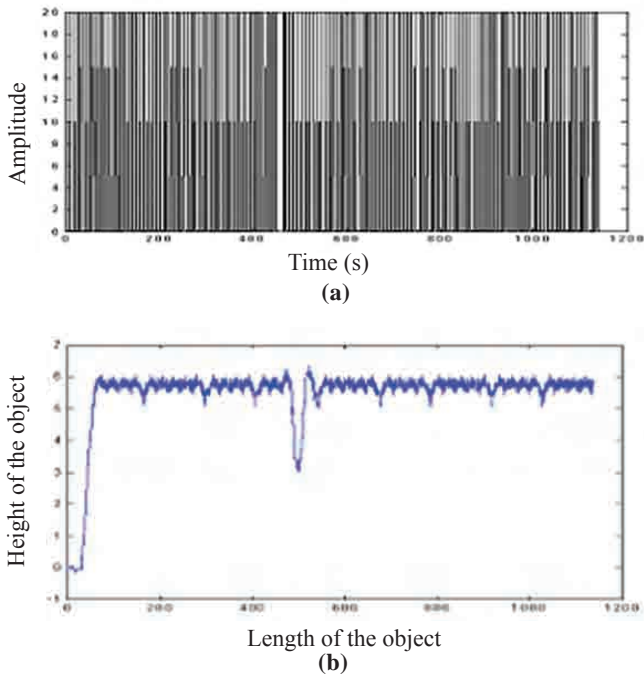


Figure 5. (a) Time series from simulation and (b) Profile function from Fig (a).

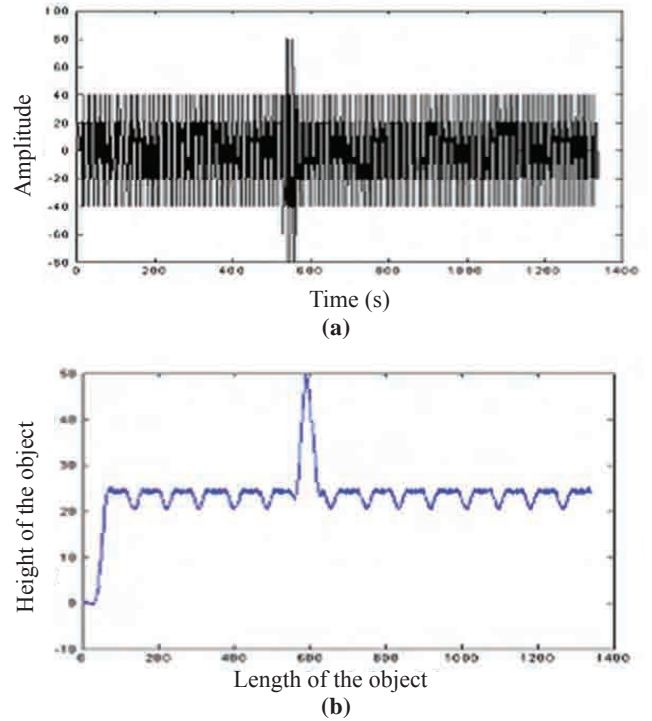


Figure 6. (a) Time series from simulation and (b) Profile function from Fig (a).

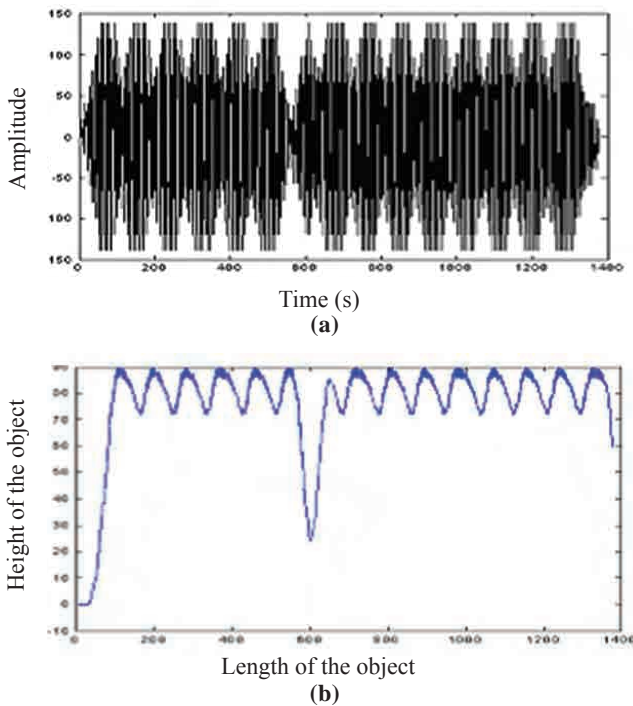


Figure 7. (a) Time series from simulation and (b) Profile function from Fig (a).

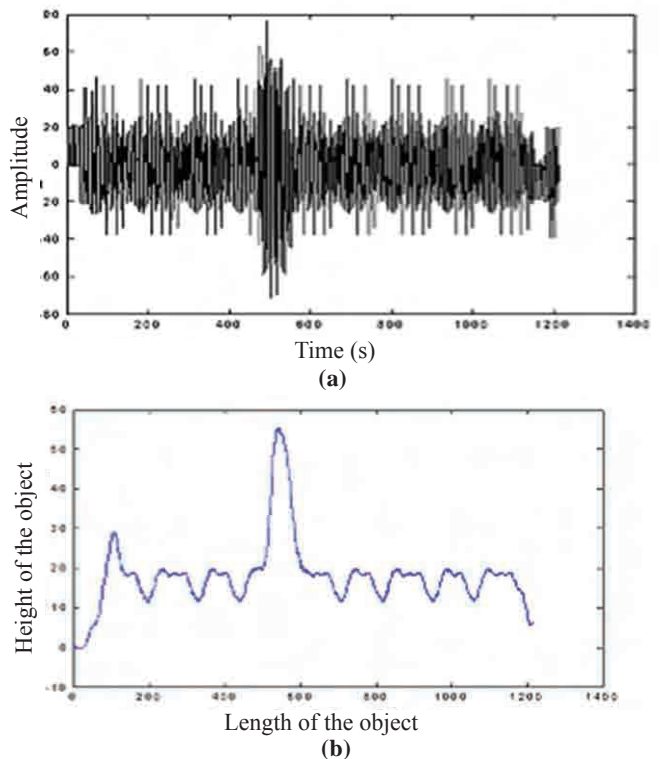


Figure 8. (a) Time series from simulation and (b) Profile function from Fig (a).

used 4000 x 200.

From results, it is clear that the computational technique can be used in any shape of the object. However, function for profile extraction most suited on impulse incidence may not be good for pulse of definite time, even though shape of object can be made out visibly. From the above results, it is also observed that shorter pulse gives the better definition than wide pulse.

Results also reveal improvement in the extracted profile by increasing the sampling rate (time resolution) and number of elements as shown in Fig. 9(b).

An experiment was conducted placing an object in

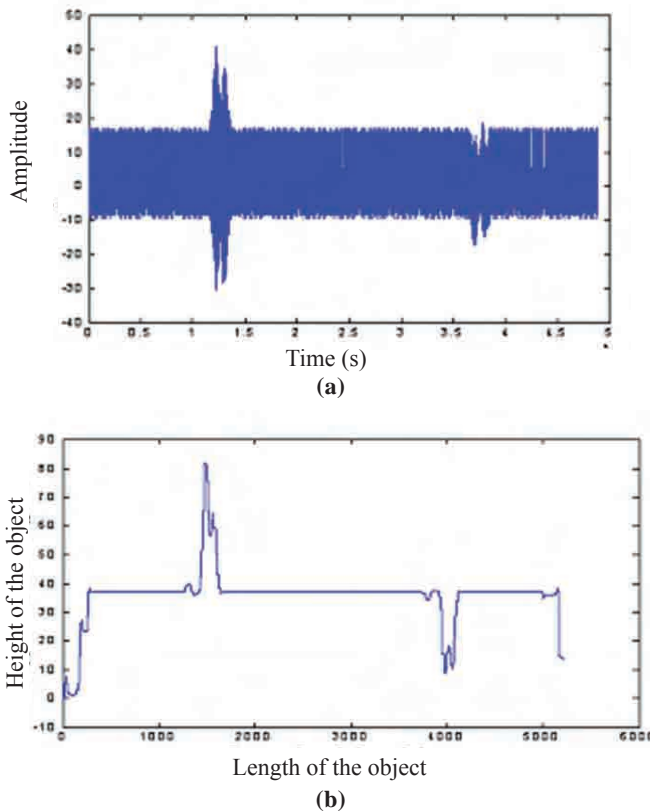


Figure 9. (a) Time series from simulation, and (b) Profile function from Fig (a).

acoustic tank. length of the tank is 50 m breadth of the tank is 18 m and depth of the tank is 20 m The tank had two moveable platforms and both are fitted with turn tables. The object was fabricated from steel, as per shape in Fig. 10(a). The size of the object has been 1.0 m x 0.4 m, with a projection of 15 cm x 15 cm. The object was held with a holding rod attached to the turn table. The unit was lowered to a depth of five meters. The projector was lowered from the second platform. The receiving hydrophone was attached to the turn table of second platform the projector and receiver are also lowered to the same depth of five meters as that of the object. Transmission angle $\theta_1 = 85^\circ$ and receiver angle $\theta_2 = 60^\circ$ were set up with respect to the object.

A pulse of 20 cycles duration, with frequency of 200 kHz was set as transmit signal. The receiver output was amplified and captured on an oscilloscope. Reflected signal was selected and recorded by appropriately setting the time, with respect to the trigger from the transmission unit. The sampling time is set as $0.1 \mu\text{s}$ per sample. The decimated time series is given in Fig. 10(c). The 'x-axis' corresponds to time, given as sample number time per sample is $0.5 \mu\text{s}$ (re-sampled by a factor of 5). And 'y-axis' corresponds to amplitude of the signal at the receiver. The time series of similar object simulated with FETD is given in Fig. 10(b). The 'x-axis' corresponds to time, given as sample number, with sampling time is set as $10 \mu\text{s}$ per sample. The 'y-axis' corresponds to amplitude of the signal at the receiver good similarity is seen with experimental result of the scaled model however minor differences may be due to

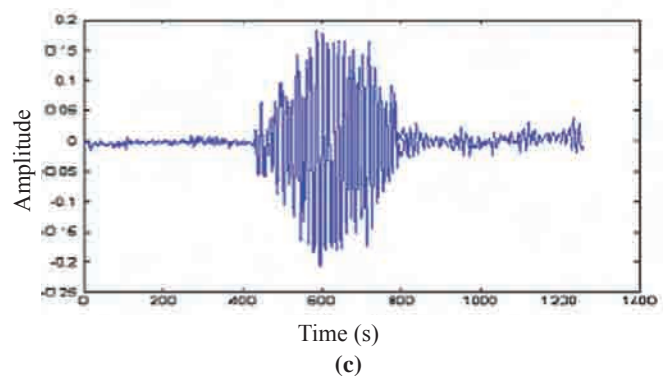
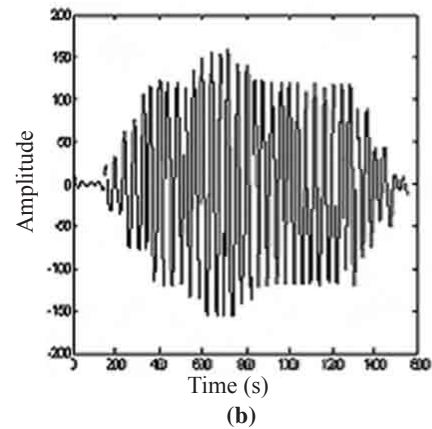
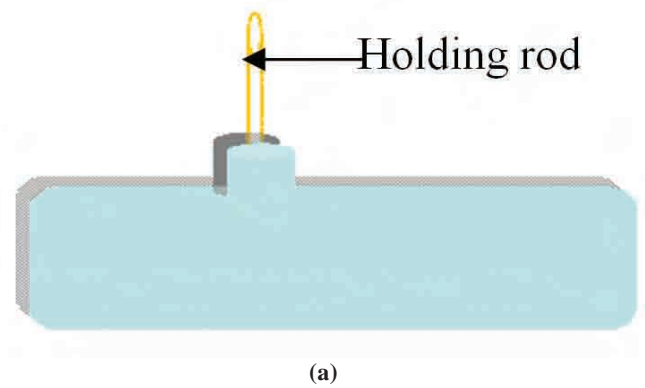


Figure 10. (a) Shape is used for experiment, (b) Time series from simulation, and (c) Time series from experiment.

the holding rod and sampling of the signal in the experiment setup. The signal amplitude in the experiment is scaled by the sensitivity of the hydrophone as seen in the Fig. 10(c).

5. CONCLUSION

Finite element time domain method is used for generating the forward scatter. The results obtained from numerical computation technique is evaluated for simulation of forward scatter for inverse scattering applications. The study indicates that,

- The discretisation is dependent on the curvature or on the feature sizes of the object, to be identified
- The sampling frequency is dependent on the spatial sampling and on the sound velocity.

- The pulse frequency is also dependent on the feature sizes to be identified. Evaluation for different pulse parameters is carried out by comparing the profile function extracted with that obtained by with single cycle (phase starting from -90° and ending with $+90^\circ$).
- The RMS error for the minimum required frequency was approximately 10%
- Doubling the frequency has reduced the RMS error to 5%.
- Increasing the pulse width has resulted in the elongation of the object length and required normalization by pulse length to estimate the size of the object.
- Profile extraction on wide pulse has to be carried out by different technique, as the scatter has the effect of multiple profiles of the object superposed and the time series thus obtained was smeared profile.
- The RMS error for the broad band (LFM and SFM) pulse order of 1%, and was less than for the narrowband pulse (7%). This is also evident from the pulse length variation.
- In bi-static mode the time series was elongated. However, variation in signal strength is observed for different angles (corresponding to beam pattern). Except for this the observations were similar to mono static observations .

The accuracy of the simulations with medium grid sizes is sufficient for inverse applications. The grid size need not be very high and depends only on the feature sizes of the object. A variable grid may be attempted where the curvatures of the body can be approximated by plane surface. This technique is mainly for computing forward scatter for inverse scattering applications. This may also has applications in generating forward scatter of very narrow and wide band signals of any pulse type and any object shape.

ACKNOWLEDGEMENT

The authors gratefully acknowledge the support of Director, NPOL, and for the permission to publish this work. The authors also acknowledge the support of Vice Chancellor, DIAT (DU), Pune for the support and encouragement.

REFERENCES

1. Young, J.D. Radar imaging from ramp response signature, *IEEE Trans. Antennas Propagation*. 1976, **24**(3), 276-282.
2. Zhang, X.M.; Wel, Li, & Liu, G.R. A new technique in ramp response for acoustic imaging of underwater objects. *Applied Acoustics*, 2002, **63**(4), 453- 465.
3. Li, Wel; Liu, G.R. & Zhang, X.M. Size identification of underwater objects from back scattering signals of arbitrary looking angles. *J. Comput. Acoust.* 2004, **12**(3), 301-17.
4. Waterman, P.C. New formulation of acoustic scattering. *J. Acoust. Soc. Am.*, 1969, **45**(6), 1417-1429.
5. Waterman, P.C. T-matrix methods in acoustic scattering. *J. Acoust. Soc. Am.*, 2009, **125**(1), 42-51.
6. Varadan, V.V. & Varadan, V.K. Scattering matrix for elastic wave. III. Application to spheroids. *J. Acoust. Soc. Am.*, 1979, **65**(4), 896-905.
7. Kennaugh, E.M. & Moffatt, D.L. Transient and impulse response approximations. *Proceedings, IEEE* 1965, **53**(8), 893-901.
8. Bodo, Nolte.; Ingo, Schafer.; Jan, Ehrlich, Martin.; Ochmann, Ralf, Burgschweiger & Steffen, Marburg. Numerical methods for wave scattering phenomena by means of differential boundary integral formulations. *J. comput. Acoust.* 2007, **15**(04), 495-529.
9. Filippi, P. ; Habault, D.; Lefebvre, J.P. & Bergassoli, A. Acoustics: Basic physics, theory and methods. Academic Press, San Diego, London, 1999
10. Ochmann, M. & Mechel, F.P. Analytical and numerical methods in acoustics in *Formulas Acoustics*. Edited by F. P. Mechel. Springer-Verlag, Berlin, Heidelberg, 2002.
11. Junger, M.C. & Feit, D. Sound, structures, and their interaction. Acoustical Society America, American Inst. Physics, 1993.
12. Bounaim, A.; Holm, S.; Chen, W. & Odegard, A. Sensitivity of the ultrasonic CARI technique for breast tumor detection using a FETD scheme. *Ultrasonics* 2004, **42**(8), 919-925.
13. Li, Wel.; Liu, G.R. & Varadan, V.K. Acoustical imaging of underwater objects using the bi -static ramp response signals. *Smart Mater. Struc.*, 2004, **13**(1), 169–174
14. Li, Wel.; Liu, G.R. & Varadan, V.K. Fredholm integral equation for the Shape reconstruction of an underwater object using backscattered ramp response signatures. *J. Acoust. Soc. Am.*, 2004, **116**(3), 1436-1445.

Contributors

Ms T. Ratna Mani received her MTech (Electronics), in 1988. She is currently working as a Scientist at Naval Physical and Oceanographic Laboratory (NPOL), Kochi. She has authored seven technical papers in international conferences and few research reports. She is a Life Member of Institute of Electronics and Telecommunications. She has a special interest in image processing. She is working on sonar systems, in the area of signal processing and under water acoustics.

Dr Raj Kumar has completed MTech and PhD in Microwave in 1992 and 1997 respectively from University of Delhi. Presently he is working as Scientist at Armament Research & Development Establishment, Pune. He has more than 190 technical papers in International Journal and conferences to his credit. His area of interest is microwave components and antennas, with special interest in numerical technique, electromagnetic analysis and simulation.

Dr O. Vijayakumar has received his PhD from Indian Institute of Science, Bangalore, in 1990. He is presently working as an Associate Director at NPOL, Kochi. He has special interest in shallow water acoustics. His areas of interest are : Under water transducers, ocean acoustics, target acoustics, and platform acoustics. He is Life Member of Acoustical Society of India.